Innovative and industrially viable approach to fabricate AlO_x rear passivated ultra-thin Cu(In, Ga)Se_2 (CIGS) solar cells.

Gizem Birant[1,2,3,a], J. de Wild[1,2,3], T. Kohl[1,2,3], D.G. Buldu[1,2,3], G. Brammertz[1,2,3], M. Meuris[1,2,3], J. Poortmans[1,3,4,5], B. Vermang[1,2,3]

[1] Institute for Material Research (IMO), Hasselt University (partner in Solliance), Agoralaan gebouw H, Diepenbeek, 3590, Belgium
[2] Imec division IMOMEC (partner in Solliance), Wetenschapspark 1, 3590 Diepenbeek, Belgium.
[3] EnergyVille, Thorpark, Poort Genk 8310 & 8320, 3600, Belgium
[4] imec (partner in Solliance), Kapeldreef 75, Leuven, 3001, Belgium
[5] Department of Electrical Engineering, KU Leuven, Kasteelpark Arenberg 10, 3001 Heverlee, Belgium
[a] gizem.birant@imec.be

Abstract

In this work, an industrially viable and novel rear surface passivation approach for Copper Indium Gallium di-Selenide, Cu(In, Ga)Se_2, CIGS, ultra-thin (500nm) solar cells is developed. The passivation layer was deposited by atomic layer deposition (ALD), and an alkali treatment was applied via spin coating. It was observed that selenization of the samples is required to create contact openings. The openings were visualized by SEM, and these results were supported by EDS. The impact of the oxide layer's thickness, as well as the alkali solution's molarity, was studied. Solar cells were produced for the optimal combination of these two parameters. As a result, with a relative 13% increase, the highest V_{oc} of 623mV was achieved. Hence, the efficiency of the passivated solar cell was relatively increased by one-third, by using an industrially feasible, fast, and repeatable technique.

1. Introduction

Today, one of the most efficient thin-film photovoltaic (PV) technology is CIGS multi-crystalline thin-film solar cells (Green et al., 2020). In order to compete with other solar cell technologies, the production costs should be reduced, and the structure should be simplified. To make cheaper solar cells, reducing the thickness of the absorber layer is one solution. However, reducing the thickness of the absorber layer has drawbacks like incomplete absorption and increased back-contact recombination, both resulting in power conversion efficiency losses (Naghavi et al., 2016), (Umehara et al., 2016). One solution is to implement a rear surface passivation layer, which has the potential to reduce rear surface recombination velocity and increase rear internal reflection (Poncelet et al., 2018). However, CIGS solar cells generally benefit from the sodium (Na) coming from the soda-lime glass substrate (Li et al., 2019), (Rudmann, 2004). Usage of a dielectric layer at the rear surface, such as alumina (Al_2O_3) which is an ideal passivation layer (Groner et al., 2002), (Poncelet et al., 2017), unfortunately, acts as an electron and diffusion barrier layer, and thus prevents current flow and the Na diffusion. In order to overcome these problems, there needs to be contact openings in this passivation layer. In reference (Vermang et al., 2014b), the rear surface passivation technique used for silicon (Si) solar cells was implemented to CIGS solar cells. In that study, Al_2O_3 was

used as the rear surface passivation layer, and nano-sized point contact openings were realized via chemical bath deposited CdS nanoparticles (Vermang et al., 2014b). Over the years, many research groups developed and applied different techniques to generate these openings in various dielectric layers, see (Birant et al., 2019). Almost all of the proven methods – e.g., using nanoparticles, e-beam or nano-imprint lithography – are well controlled, but also expensive, time-consuming or not applicable for larger areas, see (Necas and Klapetek, 2012), (Vermang et al., 2015) and (Yin et al., 2017).

D. Ledinek et al. previously proposed using a very thin layer of Al_2O_3 as rear surface passivation in combination with NaF evaporation to enhance the electrical characteristics of CIGS solar cells. In their study, the surface passivation layer is claimed to have a porous structure that allows direct contact between Mo and CIGS, and they supported their claims with TEM and XPS analysis (Ledinek et al., 2018). The proposed method in our study is to spin-coat the NaF on top of the Al_2O_3 passivation layer, which will generate contact openings during selenization. The generated contact openings were visualized by SEM prior to and after CIGS deposition. The aim is to prove that by using a simple, cost-effective, and fast process, it is possible to passivate the rear surface of ultra-thin CIGS solar cells, and hence, increase the efficiency, i.e., make it cheaper and industrially feasible.

2. Experimental details:

In this section, the implementation of the novel rear surface passivation approach into the standard solar cell structure is explained. The proposed method is to spin-coat sodium fluoride (NaF) on top of the Al_2O_3 passivation layer to generate the contact openings during selenization. Al_2O_3 passivation layer was deposited through atomic layer deposition (ALD) at 300°C. During the depositions, trimethylaluminum (TMA) was used as the precursor, and H_2O used as the reactant. The nm/cycle rate was calculated to be 0.17, by measuring the Al_2O_3 thickness on Mo with ellipsometry and assuming a constant growth rate with time. The proposed rear surface passivation approach is integrated into the standard stack: SLG/Mo/AlOx/CIGS/CdS/i-ZnO/ZnO:Al/Ni-Ag-Ni grids, where solar cell devices have ultrathin (500 nm), single-stage and ungraded, i.e. without Ga-grading, CIGS absorber layers with ([Cu]/([Ga] + [In]) = 0.83 and ([Ga]/([Ga] +[In]) = 0.33, with active area of 0.5cm^2. In this study, a flat Ga profile was preferred to eliminate reciprocal rear surface passivation effects of Ga-grading (Vermang et al., 2014b), (de Wild et al., 2019).

Table-1 Overview of all steps required to produce sample Set 1 and Set 2

Step	Sample Set 1	Sample Set 2
1	Substrate cleaning	Substrate cleaning
2	***Al_2O_3 passivation layer deposition (2nm-10nm)***	Al_2O_3 passivation layer deposition (6nm)
3	NaF spin coating (0.4M)	***NaF spin coating (0.2M-0.4M)***
4	Selenization	Selenization

In order to identify the optimal parameters, two sets of samples were prepared: altering, first, the thickness of the dielectric layer (Set 1), and second the molarity of the alkali solution (Set 2); see Table-1 and Figure-1. For both sets, and for each parameter, two different samples were produced: one for characterization and one for solar cell production. As the substrate, 3mm thick soda-lime glass (SLG) with Si(O, N) barrier layer, which has 300nm molybdenum (Mo) as the rear contact, was used.

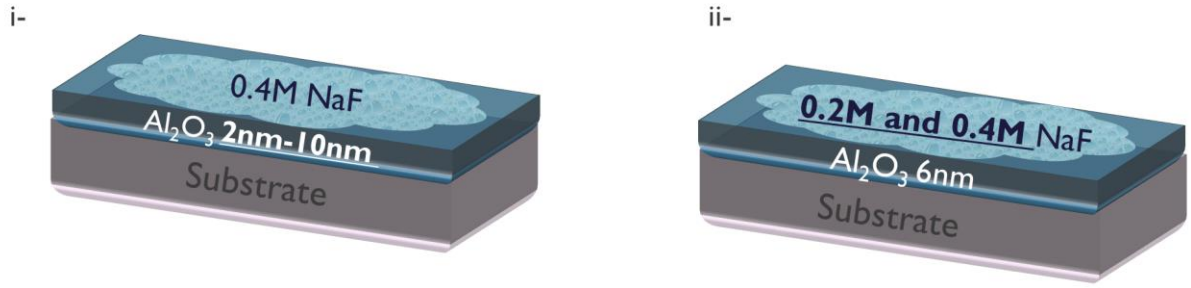

Figure 1 Sketch of the two sets of samples with altering i- Al_2O_3 thickness and ii- NaF molarity; to investigate their effects on passivation characteristics and openings.

For Set 1, five different Al_2O_3 layer thicknesses were tested, starting from 2nm and ending with 10nm, by 2nm steps. Following the Al_2O_3 depositions, 0.4M NaF was spin-coated on those layers. Characterization samples were selenized at 540°C, for 10 minutes, in order to mimic the absorber layer deposition environment. For selenization, a quad-elliptical radiant heating chamber and pure selenium particles were used. This process has occurred under a vacuum. To monitor the formation of the openings, characterization samples underwent several characterization steps. As a first step, scanning electron microscopy (SEM) imaging and energy-dispersive X-ray spectroscopy (EDS) analysis was done with a Tescan and Bruker SEM. In order to calculate the density of the opening-like structures, a data analysis software named Gwyddion was used. This software can analyze and compare the height difference between the two layers by using SEM images (Necas and Klapetek, 2012). In our case, it spots the height difference between the alumina layer and the molybdenum back contact and gives the percentage of the contact openings. An example of the Gwyddion analysis is shown in Figure-2-a. We used three different SEM pictures with varying magnifications for each sample, and use the arithmetic average of those three images while calculating the surface coverage (SC) ratios.

In order to decide the optimal thickness of the dielectric layer, samples that were completed as solar cells were used. According to the IV results, the optimal thickness was chosen as 6nm. Concerning the molarity of the NaF solution, i.e., Set 2, two different molarities were tested, 0.2M and 0.4M, with a 6nm Al_2O_3 layer. Also, regarding the necessity of this treatment, samples without any alkali treatment, i.e., 0 M condition, were prepared. Similar to Set 1, these samples also underwent the same characterization steps, and 0.4M was chosen as the optimal molarity for our approach. Exact reasons why we chose the thickness and the molarity as 6 nm and 0.4M, respectively, will be shared in the following section.

Production steps of the reference and passivated solar cells are shared in Table-2. For the passivated solar cell, the aforementioned optimal parameters were used, and the detailed explanation of the steps for the reference sample can be found in (de Wild et al., 2019).

The completed solar cells were characterized by JV measurement under AM 1.5 illumination. The Voc, Jsc, FF, and efficiency were derived from the JV curves. Twelve cells were measured for reference and passivated samples, and the arithmetic average results are shared in Table-3. The values for saturated current density (J_0), shunt and series resistances (Rsh and Rs) are calculated from the dark JV measurement using a MATLAB routine. J_0 values are extracted from the JV curve, which is corrected for Rs and Rsh, with a 1-diode model.

Table-2 Overview of all steps required to produce reference Cu(In, Ga)Se_2 solar cells and Al_2O_3 rear surface passivated cells with contacts.

Step	**Description**	
	Reference	**Passivated**
1	Substrate cleaning	Substrate cleaning
2		***Al_2O_3 passivation layer deposition***
3	NaF spin coating	NaF spin coating
4	1 stage ultra-thin (500 nm) CIGS absorber co-evaporation	1 stage ultra-thin (500 nm) CIGS absorber co-evaporation
5	CBD CdS buffer deposition	CBD CdS buffer deposition
6	i-ZnO and ZnO:Al window sputtering	i-ZnO and ZnO:Al window sputtering
7	Ni/Al/Ni front contact evaporation	Ni/Al/Ni front contact evaporation

EQE was measured under dark conditions and scanned through the wavelength interval of 350-1300nm in 5nm steps. For the passivated sample, Jsc values were extracted from the EQE, and the efficiencies recalculated accordingly. PL and TRPL measurements were carried out in a photo spectrometer from Picoquant with a TimeHarp 260 single-photon counter for the time-resolved measurements. The excitation intensity is approximately 0.2 W cm^{-2}, the repetition rate is 3 MHz, and the wavelength is 532nm.

3. Results and discussion:

3.1 Creation of the contact openings:

In order to interpret the effect of NaF spin-coating on the alumina passivation layer during selenization, two characterization sample sets were used as described above. To monitor the results of this process, SEM imaging was done before and after this step, and results were supported with EDS analysis, see Figure-2-b. In the end, it was experimentally proven that, during the selenization, in certain cases, contact openings are formed in the passivation layer. The impact of the thickness of the dielectric layer and the molarity of the alkali solution on the density and size of the contact openings was also investigated, see Figure-3-a. By considering the change in the surface coverage ratios as well as the shape and the size of the openings, samples that were finished as solar cells were used to assess the impact of this difference on open-circuit voltage, Voc.

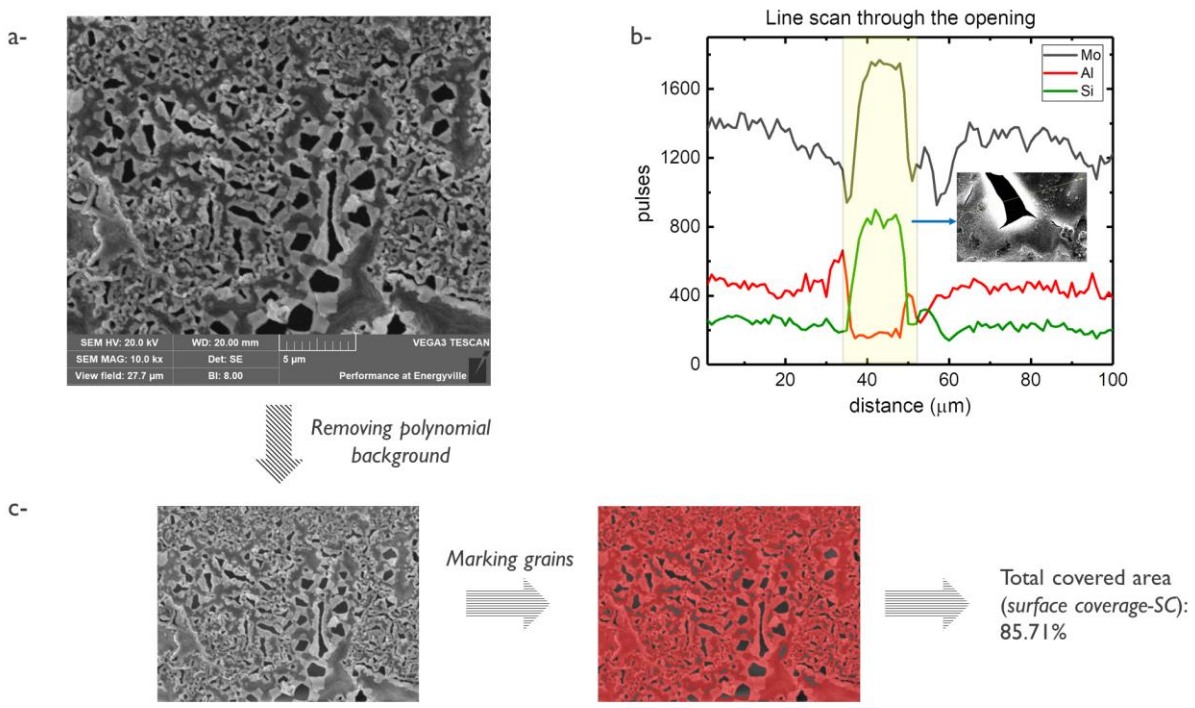

Figure 2 a-SEM picture of the optimal sample after selenization and b- EDS line scan to prove the existence of the openings in the dielectric layer (inset SEM picture of the analyzed sample) and c- example of Gwyddion analysis with calculated surface coverage ratio.

As can be seen from Fig.3-b, there is an inverse relation between Voc and the SC. The discussion part for this graph is divided into two subsections: 3.1.1- effect of the thickness of the Al_2O_3 layer and 3.1.2- effect of the molarity of the alkali solution. In the end, there is section iii, which will contain the discussion associated with the solar cells prepared with the optimal conditions decided according to subsections 3.1-a and 3.1-b.

3.1.1 Effect of the thickness of the alumina layer, Set 1:

For this set, in order to monitor the effect of the thickness of the Al_2O_3 layer, we kept the molarity of the alkali solution as 0.4M for all of the samples. As can be seen from Fig.3-a, for 8nm and 10nm thick alumina layers, we could not detect any opening like structure. On the other hand, for 2nm, 4nm, and 6nm thick alumina layers, we were able to observe openings in the alumina layer. For those samples, the surface coverage ratios were calculated with the help of Gwyddion software, as described in Fig.2-c. If Fig.3.b is investigated further in terms of the thickness of the Al_2O_3 layer, it can be seen that until the 8nm thick dielectric layer, the Voc is improved compared to the reference. However, for 8nm and 10nm thick Al_2O_3 layer, the Voc is worse than the rest of the Set-1, including the reference. This information is vital for us to understand that, with our novel contacting approach, thicknesses over 6nm is not suitable for rear surface passivation.

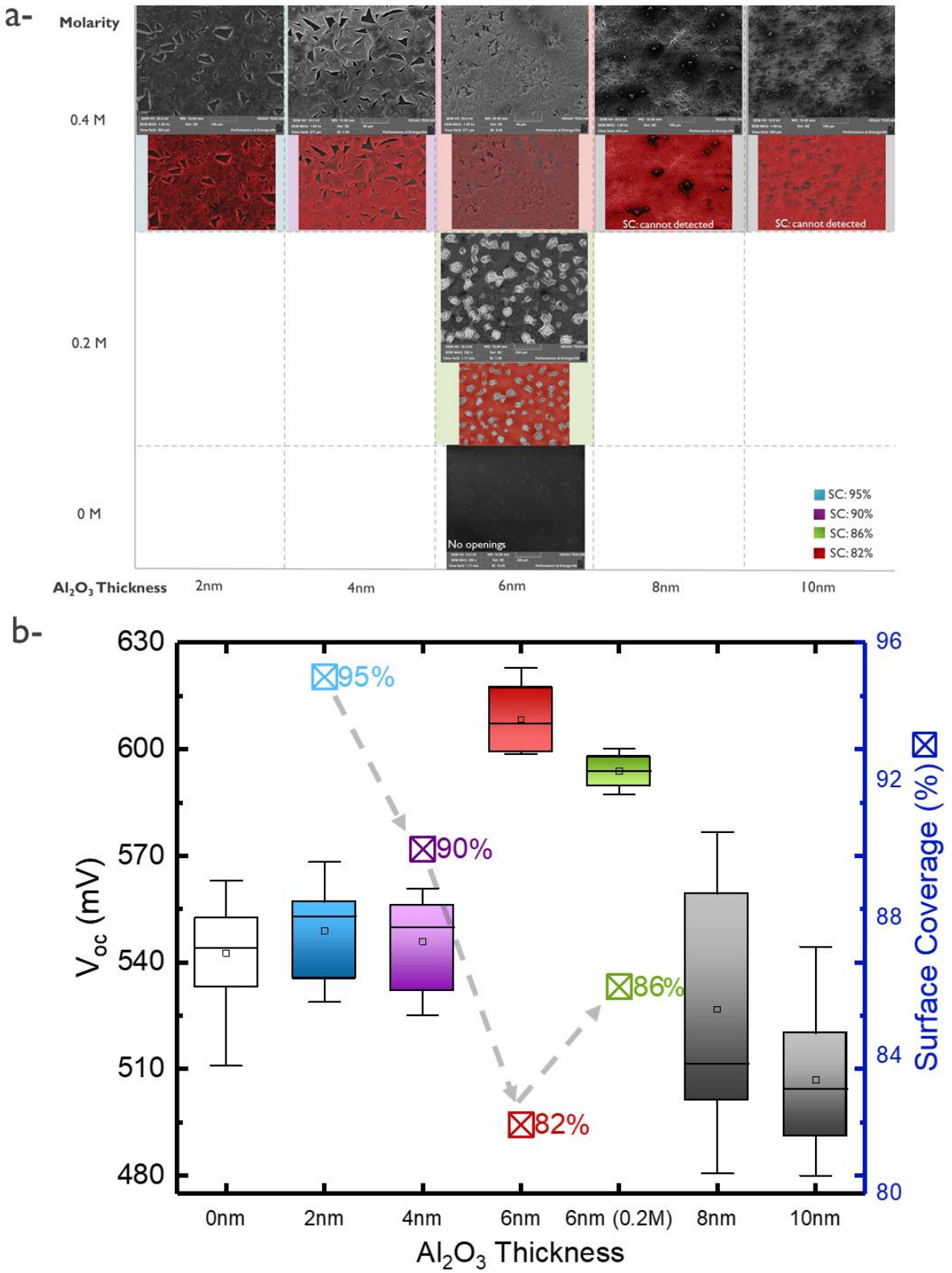

Figure 3 a-Molarity vs. thickness of the aluminum oxide layer with insets of SEM images, Gwyddion masks and surface coverage ratios of samples belongs to Set 1 and Set 2, and b-Open circuit voltage and surface coverage ratios vs. thickness of the aluminum oxide layer for the same set of samples; box charts represents the Voc and boxes represents the SC (%). *The arrows are given to emphasize the inverse relation between Voc and SC in terms of* Al_2O_3 *thickness.*

When we compare our surface coverage (SC) results with other groups, we realized a slight difference. In (Casper et al., 2016), they studied rear surface passivation of ultra-thin CIGS solar cell, by using 25nm and 50nm thick Al_2O_3 as the passivation layer, and the contact openings were realized by lithography, i.e., they had controlled size and distribution for the openings. They experimentally proved that 90% surface coverage gave the best Voc. In (Vermang et al., 2014a), on the other hand, it was mentioned that the 5% contact opening area, i.e., 95% surface coverage, in 5nm thick $Al2O_3$ layer is sufficient for passivation. In our case, we got the best Voc from 6nm thick Al_2O_3, i.e., 83% SC (Fig.3-a). The reason for this difference can be explained by our novel approach. Since the size and the distribution of the openings are reasonably random, and not yet controllable, it is reasonable to have slightly different results from the literature. The detailed solar cell results will be shared and discussed in the following section. The JV results showed that for 2nm (95% SC) and 4nm (90% SC) thick layers, there was a little enhancement in Voc values as compared to the reference, i.e., unpassivated solar cell, but it was not as significant as a 6nm (83% SC) thick layer. Since the effect of the rear surface passivation reveals itself as an increased diffusion length of the minority carriers due to the created field effect, the difference in these results can be explained by the insufficient thickness of the dielectric layer and the non-optimized contacting approach (Kotipalli, 2016). For 8nm and 10nm thick layers, on the other hand, the current was almost completely blocked, and the passivation layer acted as a barrier layer. The JV curves of those samples showed us that the sample with an 8nm thick Al_2O_3 layer has suffered from low shunt resistance, and the sample with a 10nm thick Al_2O_3 layer had high series resistance, both results in low FF, hence low power conversion efficiency. (Supporting Figure 1) Therefore, we proved that 8nm and 10nm are too thick for described alkali treatment to make sufficient openings with our approach, and consequently, we decided to use a 6nm thick alumina layer for further experiments.

3.1.2 Effect of the molarity of the alkali solution, Set 2:

After optimizing the thickness of the passivation layer to 6nm, we investigated the necessity of the alkali treatment. To do so, two samples were prepared, one without any alkali treatment and one with a 0.2M NaF solution. As can be seen from Figure-3-a, if we do not use any alkali solution, there will be no opening-like structures in the alumina layer. On the other hand, for the 0.2M NaF solution, we were able to detect and analyze the openings. There is a slight difference in SC ratios between 0.2M (86.5% SC) and 0.4M (83% SC) NaF solutions. However, if the solar cell parameters, especially the Voc, are compared, it is safe to say that 0.4M NaF works better than 0.2M NaF, see Figure-3-b.

According to the JV measurement, it is clear that the alkali treatment is necessary since the current is completely blocked, resulting in diode like response under illumination, for the solar cell that has no alkali treatment. Besides, for 0.4M NaF, as told earlier, we achieved better solar cell characteristics in comparison to 0.2M NaF. The FF, for instance, is noticeably lower for 0.2M NaF sample, 20% less than 0.4M NaF sample, which was resulting in lower power conversion efficiency. (Supporting Figure 2) This can be explained by the lack of contact openings due to less alkali salt crystal and/or lack of Na supply due to low concentration. Hence, we decided to use a 0.4M NaF solution from this point forward.

3.1.3 Solar cells prepared with optimal conditions:

After we validated our approach regarding the openings with the help of two sets of characterization samples, the next step was to prove that our assumption is valid for finished solar cells. We prepared a sample with the optimal conditions again. The first aim is to show the process's repeatability, and the second aim is to use that sample for detailed electrical and optical analysis. After completing the measurements, we picked the solar cell with the highest efficiency, and then made a scratch with the help of a tweezer to remove the window layer and the absorber layer. The aim is to prove that the contact openings are realized in the dielectric layer during CIGS absorber layer deposition. Since we only mimicked the environment for characterization samples, it is always possible that during the actual deposition, conditions can slightly differ. After we made the scratch, we were able to prove that there were contact openings created in the passivation layer for a finished solar cell as well, by using SEM and EDS measurements. (Supporting Figure 3) As a result, we proved that with our novel approach, contact openings could be realized in the dielectric passivation layer with a fast and cost-effective technique.

3.2 Electrical and optical analysis of the solar cell devices produced with optimal parameters:

In this section, we present the results of the solar simulator, EQE, and TRPL. The results of these measurements will be shared and discussed in detail.

The arithmetic average of standard solar cell parameters for the 12 best cells for passivated and reference samples is given in Table-3. Further, two passivated cells that have the best efficiency and the best Voc when compared to the other cells are shared as well.

The addition of the passivation layer with contact openings leads to an increase in nearly all solar cell parameters compared to standard unpassivated solar cells. We extracted the Jsc values from the EQE for the best two solar cells only, in order to avoid potential errors caused by the grids or scribing. Then, the power conversion efficiency values for those two best cells are recalculated (Table-3). If we compare the Jsc value for the average passivated solar cells and Jsc value that is extracted from the EQE for the best cells, we noticed a 5mA difference between those values, see Table-3. The probable cause for this difference is explained in detail in (Scheer and Schock, 2011).

As shared in Table-3, by the addition of a passivation layer with contact openings through an easy and cost-effective way, we reached Voc of 623mV with ultra-thin single-stage CIGS solar cells. If we examined even further, due to the 14% relative increase in open-circuit voltage, i.e., from 536mV to 608mV, the power conversion efficiency of the passivated sample gained a 24% relative increase, i.e., from 5.2% to 7.2%, for the average of twelve cells. Furthermore, by using the extracted current values from EQE, i.e., corrected Jsc, we achieved 9.8% power conversion efficiency.

Table-3 JV parameter comparison between reference (bare) and passivated ultrathin CIGS solar cells. (average of 12 cells) Further, JV parameters of the cells that have the best efficiency and open-circuit voltage values for passivated solar cells. **Jsc values extracted from EQE and the power conversion efficiencies recalculated accordingly.*

	Number of cells	Jsc (mA/cm^2)	Voc (mV)	FF (%)	Eta (%)
Reference-**Average**	12	20.9 ± 2.3	536 ± 28.1	51.8 ± 6.6	5.8 ± 1.1
Passivated-**Average**	12	19.9 ± 1.63	608 ±8.9	59.6 ± 1.77	7.2 ± 0.7
Passivated-Best Eff.	1	**25.1***	617.01	62.2	**9.8***
Passivated-Best Voc	1	**23.6***	622.84	56.9	**8.4***

The rear surface passivation effect can easily be explored by examining the differences between reference and passivated solar cells' Voc values. To this effect, the following simplified equation is used:

$$V_{oc} \approx \frac{k_B T}{q} \ln\left(\frac{J_{ph}}{J_0}\right) \qquad \text{Eq.1}$$

where J_{ph} is equal to short circuit current in an ideal case. Since the variation in J_{ph} is generally limited, the key element that determines the change in Voc is the saturation current density. The change in saturation current density (J_0) can be in orders of magnitudes, and this change depends on the recombination in the solar cell (Smets et al., 2016). Hence, lower J_0 means lower recombination, and eventually higher Voc. The addition of the aluminum oxide dielectric layer in combination with sodium fluoride decreases the J_0 noticeably, and causes a significant increase in Voc, see Table-4.

For further investigation, we update the Eq.1 to calculate the open-circuit voltage difference (ΔV_{oc}) between reference and passivated solar cells:

$$\Delta V_{oc} \approx \frac{k_B T}{q} \ln\left(\frac{J_{0,passivated}}{J_{0,reference}}\right) \qquad \text{Eq.2}$$

A random cell for reference and passivated sample, and the best efficient passivated solar cell are chosen and the measured J_0 and Voc values, ΔV_{oc} and calculated Voc values for those cells are given in Table-4.

Table 4- The saturated current density (J_0), measured open-circuit voltage (V_{oc}-m), the difference in Voc (ΔV_{oc}) (calculated from Eq.2) and the calculated open-circuit voltage (V_{oc}-c) values are given for: the reference average, the passivated average, and the passivated-best efficient solar cells.

	J_0 (mA/cm^2)	V_{oc}-m (mV)	V_{oc}-c (mV)	ΔV_{oc}
Reference- average cell	$1.72E-8$	562	-	-
Passivated-average cell	$5.63E-9$	610	652.5	90.5
Passivated-best efficient cell	$5.62E-10$	617.1	711.9	149.9

According to the Table-4, the significant decrease in the Jo results in an increase in Voc values. This increase implies that the reason for higher Voc is very likely due to reduced recombination at the rear surface. The reduced rear surface recombination should show itself clearly as an improved FF, as well (Vermang et al., 2014b), (Leilaeioun, 2018). However, our contacting approach is not optimized yet, so the increase in FF is somewhat limited. This limitation is due to the high series resistance (Rs) values for passivated solar cells. (Fig.5 a) The Rs values for passivated solar cells are significantly higher than the reference solar cells. This increase means that there is a lack of contact openings. Hence, our contacting approach needs further optimizations. In fact, after further optimizations, the calculated Voc values could be reached. If the TRPL and EQE results are investigated, it can be seen that the improvement in Voc is not related to optical enhancements, see Figure-4. The 1-Reflectance (1-R), is also given in Fig.4-b. Since the transmittance is nearly zero for our structure, 1-R can be accepted as the absorption of our solar cells. The TRPL measurement was performed on the finished solar cells. As can be seen from Fig.4-a, the passivated solar cell gave the slowest decay time. This slow decay arguably implies the reduced recombination at the rear surface. However, even for the passivated solar cell, the life-time is not at the same level as the state-of-the-art CIGS solar cells. At this point, one needs to remember that our absorber layer is ultra-thin (500nm) and non-graded. So, lower life-time values are expected.

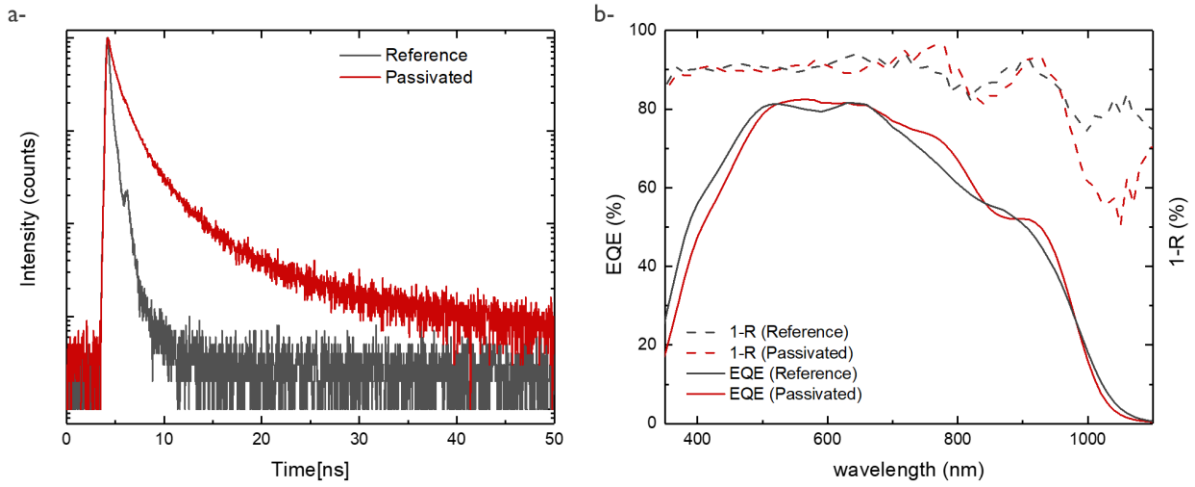

Figure 4 a-TRPL and b-smoothened EQE and 1-R of reference (black) and passivated (red) solar cells.

For passivated solar cells, the EQE response is higher for long wavelengths. One known reason for this increase is the optical enhancement due to the contact openings. The bump around 980nm for the passivated solar cell can be seen as an optical effect since a similar bump has been explained in detail for 390nm thick CIGS solar cells before, as an optical effect, see (Hegedus and Shafarman, 2004). On the other hand, the results coming from the reflectance measurement (1-R) for passivated and reference solar cells are quite similar. Hence, the increase in EQE can be associated with the rear-surface passivation effect rather than the optical enhancement.

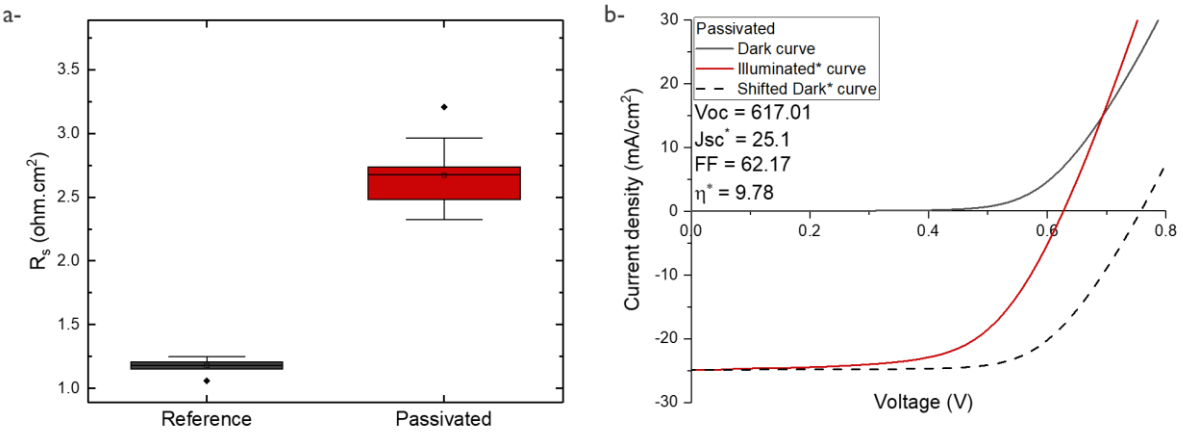

Figure 5 a- Distribution of the series resistance values for reference (black) and passivated (red) solar cells and b- JV curve for the best efficient passivated solar cell with the shifted dark curve. **Jsc and efficiency values were extracted from EQE, and the associated curves also adapted for this change.*

We also analyze the JV curve for the passivated sample to check if there are any anomalies, see Figure 5-b. Our JV curve seems to suffer from two anomalies: i-violation of superposition principle and ii-cross-over. In (Scheer and Schock, 2011), both of these anomalies and the reasons for them were discussed in detail. In our case, the most probable reasons for (i) is that

a- the boundary condition for quasi-neutral region (QNR) recombination is changed by large series resistance, or b- due to light modulated potential barrier, the change from interface recombination to Shockley Read Hall (SRH) recombination. We shifted the dark curve by Jsc and compared it with the light curve. The aim is to see the Voc without any light-induced defect and/or recombination. (Fig. 5-b) Since the FF is increasing under light, the reason for this anomaly, i.e., shifting violation, is most probably caused by high series resistance.
If we investigate the JV curve further, the second anomaly (ii) that we suffered from, the cross-over phenomenon, can be seen (Igalson et al., 2009). Several possible reasons can cause this anomaly, but the exact reason is still unknown. However, if we will be able to solve our high series resistance problem, and by doing so, overcome the violation of shifting anomaly, we will also be able to overcome the cross over phenomenon. If the shifted dark curve, i.e., the dashed curve, is followed, it is clear that it will not cross the dark curve. (Fig. 5-b) Hence, reducing the series resistance by optimizing our contacting approach will help us to overcome those anomalies in the future. As a result, we can reach higher efficiencies.

4. Conclusion and outlook:

In summary, we fabricated ultrathin rear surface passivated solar cells with an industrially viable, fast and novel process. The novelty of our process is to create the contact openings by adding NaF solution by spin coating it on the alumina passivation layer. In this way, we managed to detect the openings in the passivation layer by top-view SEM, even for the complete solar cell. Even though we are still not able to thoroughly explain the origin of these openings, it became clear that we need the alkali solution and the selenization at 540-degree Celsius. After we were convinced that we managed to create the contact openings, we altered the thickness of the passivation layer and the molarity of the alkali solution in pursuit of finding the ultimate structure for best efficiency. As a result, we decided that 6nm alumina deposition in combination with 0.4M NaF solution gives the best JV results. Hereby, we reached 623mV Voc, and for the best cell, we gained a 43% relative increase in power conversion efficiency. The main advantage of this structure is that it is easy, fast and applicable to larger areas. Considering that spin-coating is not an industrially feasible technique, instead of this, other industrially feasible coating techniques, for example, slot dye technique, could be used for sodium fluoride deposition. Even though this process is not as controllable as more standard techniques, upon the repetition of our experiment, we obtained very similar results. So, it is safe to say that the alterations, i.e. non-controllable elements, do not affect the efficiency significantly. Moreover, it is possible to apply this structure to the front surface of CIGS solar cells. The next step is to investigate further the chemistry and physics behind the creation of the openings, and then optimize the process. After that, we believe that the calculated Voc values can be reached by reducing the series resistance.

Acknowledgment:
This work received funding from the European Unions H2020 research and innovation program under grant agreement No. 715027.

References:

Birant, G., Wild, J. De, Meuris, M., Poortmans, J., Vermang, B., Pv, S., 2019. Dielectric-Based Rear Surface Passivation Approaches for Cu (In , Ga) Se 2 Solar Cells — A Review. Appl. Sci. 9. https://doi.org/10.3390/app9040677

Casper, P., Hünig, R., Gomard, G., Kiowski, O., Reitz, C., Lemmer, U., Powalla, M., Hetterich, M., 2016. Optoelectrical improvement of ultra-thin Cu (In,Ga)Se2 solar cells through microstructured MgF2 and Al2O3 back contact passivation layer. rrl Sol. 376–380. https://doi.org/10.1002/pssr.201600018

de Wild, J., Buldu, D.G., Schnabel, T., Simor, M., Kohl, T., Birant, G., Brammertz, G., Meuris, M., Poortmans, J., Vermang, B., 2019. High Voc upon KF Post-Deposition Treatment for Ultrathin Single-Stage Coevaporated Cu(In, Ga)Se2 Solar Cells. ACS Appl. Energy Mater. 2, 6102–6111. https://doi.org/10.1021/acsaem.9b01370

Green, M.A., Dunlop, E.D., Hohl-Ebinger, J., Yoshita, M., Kopidakis, N., Ho-Baillie, A.W.Y., 2020. Solar cell efficiency tables (Version 55). Prog. Photovoltaics Res. Appl. 28, 3–15. https://doi.org/10.1002/pip.3228

Groner, M.D., Elam, J.W., Fabreguette, F.H., George, S.M., 2002. Electrical characterization of thin Al2O3 films grown by atomic layer deposition on silicon and various metal substrates. Thin Solid Films 413, 186–197.

Hegedus, S.S., Shafarman, W.N., 2004. Thin-film solar cells: device measurements and analysis. Prog. Photovoltaics Res. Appl. 12, 155–176. https://doi.org/10.1002/pip.518

Igalson, M., Zabierowski, P., Prza, D., Urbaniak, A., Edoff, M., Shafarman, W.N., 2009. Understanding defect-related issues limiting efficiency of CIGS solar cells. Sol. Energy Mater. Sol. Cells. https://doi.org/10.1016/j.solmat.2009.01.022

Kotipalli, R.V.R., 2016. Surface Passivation Effects of Aluminum Oxide on Ultra-Thin CIGS Solar Cells. Université Catholique de Louvain.

Ledinek, D., Donzel-gargand, O., Sköld, M., Keller, J., Edo, M., 2018. Effect of different Na supply methods on thin Cu(In,Ga)Se2 solar cells with Al2O3 rear passivation layers. Sol. Energy Mater. Sol. Cells 187, 160–169. https://doi.org/10.1016/j.solmat.2018.07.017

Leilaeioun, M., 2018. Fill Factor Loss Mechanisms: Analysis and Basic Understanding in Silicon Hetero-junction Solar Cells. Arizona State University.

Li, W., Yan, X., Aberle, A.G., Venkataraj, S., 2019. Effect of sodium diffusion on the properties of CIGS solar absorbers prepared using elemental Se in a two-step process. Sci. Rep. 1–11. https://doi.org/10.1038/s41598-019-39283-2

Naghavi, N., Mollica, F., Goffard, J., Posada, J., Duchatelet, A., Jubault, M., Donsanti, F., Cattoni, A., Collin, S., Grand, P.., Greffet, J.., Lincot, D., 2016. Ultrathin Cu(In,Ga)Se2 based solar cells. Thin Solid Films. https://doi.org/10.1016/j.tsf.2016.11.029

Necas, D., Klapetek, P., 2012. Gwyddion : an open-source software for SPM data analysis. Cent. Eur. J. Phys. 10. https://doi.org/10.2478/s11534-011-0096-2

Poncelet, O., Kotipalli, R., Vermang, B., Macleod, A., Francis, L.A., Flandre, D., 2018. Optimisation of rear reflectance in ultra-thin CIGS solar cells towards > 20 % efficiency. Sol. Energy Mater. Sol. Cells 146, 443–452. https://doi.org/10.1016/j.solener.2017.03.001

Poncelet, O., Kotipalli, R., Vermang, B., Macleod, A., Francis, L.A., Flandre, D., 2017. Optimisation of rear reflectance in ultra-thin CIGS solar cells towards > 20 % efficiency. Sol. Energy 146, 443–452. https://doi.org/10.1016/j.solener.2017.03.001

Rudmann, D., 2004. Effects of sodium on growth and properties of Cu(In,Ga)Se2 thin films and solar cells. Swiss Federal Institute of Technology (ETH) Zurich. https://doi.org/doi.org/10.3929/ethz-a-004796411

Scheer, R., Schock, H., 2011. Chalcogenide Photovoltaics. WILEY-VCH. https://doi.org/10.1002/9783527633708

Smets, A.H.M., Jäger, K., Isabella, O., van Swaaij, R.A., Zeman, M., 2016. Solar Cell Parameters and Equivalent Circuit 9.1 External solar cell parameters. Sol. energy Phys. Eng. Photovolt. conversion, Technol. Syst. 113–121.

Umehara, T., Iinuma, S., Yamada, A., 2016. Investigation of the effects of rear surface recombination on the Cu(In,Ga)Se2 solar cell performances. Electron. Mater. Lett. 12, 479–483. https://doi.org/10.1007/s13391-016-4010-3

Vermang, B., Gao, X., Edoff, M., 2014a. Improved Rear Surface Passivation of Cu(In,Ga)Se2 Solar Cells : A Combination of an Al2O3 Rear Surface Passivation Layer and Nanosized Local Rear Point Contacts 4, 486–492. https://doi.org/10.1109/JPHOTOV.2013.2287769

Vermang, B., Timo, J., Fjällström, V., Rostvall, F., Edoff, M., Gunnarsson, R., Pilch, I., Helmersson, U., Kotipalli, R., Henry, F., Flandre, D., 2015. Highly reflective rear surface passivation design for ultra-thin Cu(In,Ga)Se2 solar cells. Thin Solid Films 582, 300–303. https://doi.org/10.1016/j.tsf.2014.10.050

Vermang, B., Wätjen, J.T., Fjällström, V., Rostvall, F., Edoff, M., Kotipalli, R., Henry, F., Flandre, D., 2014b. Employing Si solar cell technology to increase efficiency of ultra-thin Cu(In,Ga)Se 2 solar cells. Prog. Photovoltaics Res. Appl. 22, 1023–1029. https://doi.org/10.1002/pip.2527

Yin, G., Knight, M.W., Lare, M. Van, Magdalena, M., Garcia, S., Polman, A., Schmid, M., 2017. Optoelectronic Enhancement of Ultrathin CuIn1 – x Gax Se2 Solar Cells by Nanophotonic Contacts. Adv. Opt. Mater. 5. https://doi.org/10.1002/adom.201600637

Supporting Information:

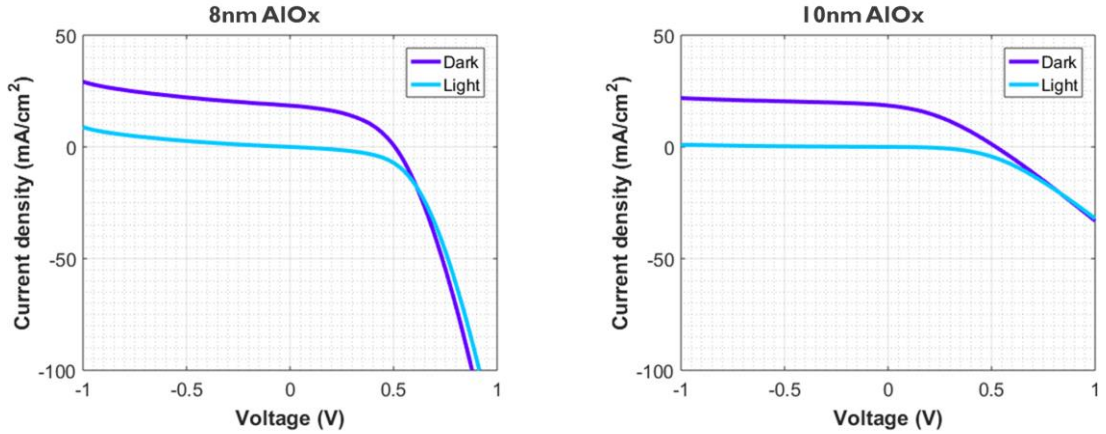

Supported Figure 1 : IV curves for samples with 8nm and 10nm AlOx layer.

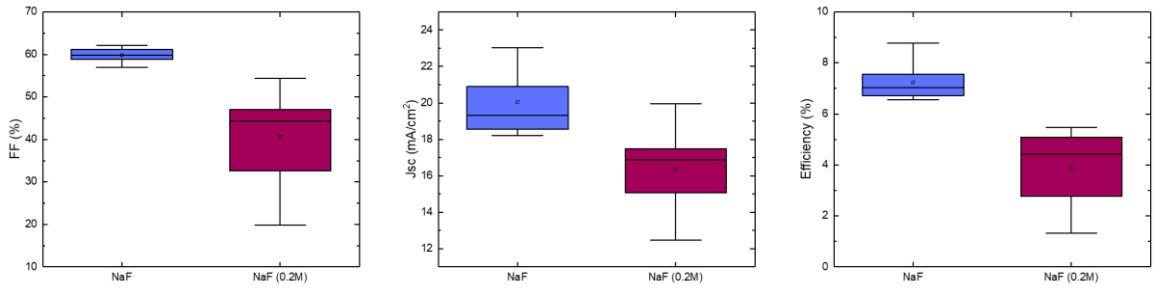

Supported Figure 2 : Comparison of the solar cell parameters for the samples with 0.4M and 0.2M NaF on top of 6nm AlOx dielectric layer.

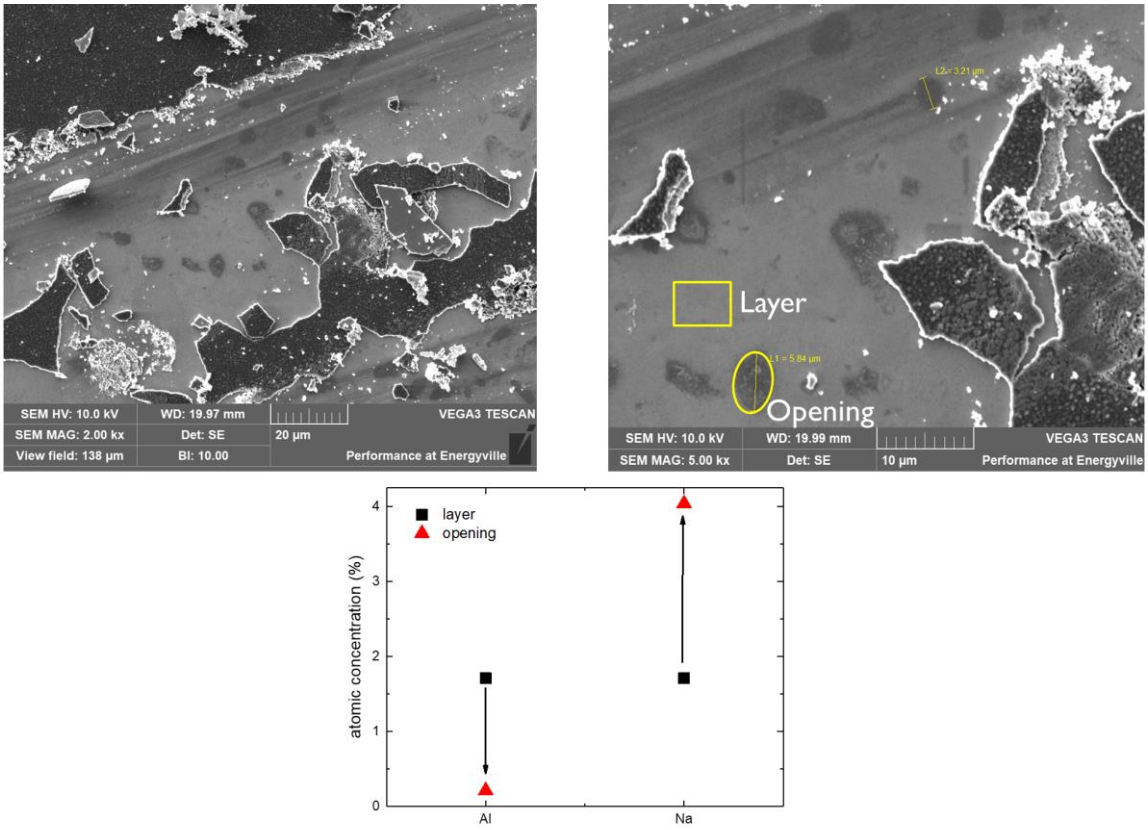

Supported Figure 3: EDS analysis and SEM pictures of openings from the complete cell structure. EDS measurement was done from layer and opening, and the atomic concentrations are shared as a graph to emphasize the change. The arrows indicate the direction of the change. As can be seen from the EDS graph, the Al signal drops nearly to zero, which means there is no Al signal through the opening. On the other hand, the Na signal increases from layer to openings. This indicates that aluminum oxide layer blocks the Na coming from the glass, and hence, from the openings, we observed higher Na signal.
Window and absorber layers removed via tweezer.